# Isolation and Characterization of a *Drosophila* Gene Essential for Early Embryonic Development and Formation of Cortical Cleavage Furrows

**Claire X. Zhang, Maxwell P. Lee, Alice D. Chen, Sheryl D. Brown, and Tao-shih Hsieh**

Department of Biochemistry, Duke University Medical Center, Durham, North Carolina 27710

***Abstract.*** We have isolated a new female sterile mutant from *Drosophila melanogaster*, which arrests the embryonic development during the transition from syncytial to cellular blastoderm. Cytological analysis of the mutant embryos indicates that pseudocleavage furrows in the syncytial blastoderm are abnormal but not completely disrupted. However, cleavage furrows during cellularization are totally disorganized, and no embryos can develop beyond this stage. Consistent with this observation, the expression of this gene peaks around the cellular blastoderm and not in any later developmental stages. Based on immunofluorescence experiments, the protein product of this gene is localized in both pseudocleavage furrows at the syncytial blastoderm and in the cleavage furrows during the cellularization stage. Sequence homology analysis demonstrates a modest, but statistically significant, similarity of this protein with the carboxyl-terminal domains of dystrophin and a family of proteins collectively known as apodystrophins. It is possible that this protein may play an essential role in organizing and maintaining a specialized cytoskeletal structure, a function also suggested for dystrophin and apodystrophins.

THE early development of the *Drosophila* embryo is completely under maternal control (Zalokar, 1976; Merrill et al., 1988; Wieschaus and Sweeton, 1988). It is characterized by rapid DNA replication and nuclear division without intervening cytokinesis (Rabinowitz, 1941; Foe and Alberts, 1983). The first eight nuclear divisions happen in the interior of the embryo. Starting from the telophase of cycle 8 and finishing at the interphase of cycle 10, the majority of nuclei migrate synchronously toward the cortex of embryo (Foe and Alberts, 1983; for review see Foe et al., 1993). At cycle 9, ~10 nuclei migrate ahead of the main body of nuclei and reach the posterior end to form pole cells, the precursors of germ line cells. The cortical nuclei then undergo four synchronous divisions as a regularly spaced monolayer underneath the plasma membrane. These four nuclear divisions, cycles 10 to 13, are termed the syncytial blastoderm stage. Cellularization commences at the beginning of interphase of cycle 14, when zygotic machinery starts to take over embryogenesis. During the ensuing period of ~45 min, membrane biogenesis coincides with the formation of cleavage furrows and allows ~6,000 cortical nuclei to be enclosed with plasma membrane. Gastrulation occurs immediately after the completion of the cellularization process.

The precision and order of these early developmental processes are under the control of and dependent upon the cytoskeletal structure of embryos. During *Drosophila* early embryogenesis when all nuclear divisions occur in a syncytium, cytoskeletal organization is especially important in the formation of a highly regular structure of cortical nuclei (for review see Fyrberg and Goldstein, 1990; Schejter and Wieschaus, 1993). In preblastoderm stages, nuclei divide in the center of the embryo, and each nucleus is surrounded by a special domain enriched in cytoskeletal elements. The cytoskeleton is also localized in a cortical layer beneath the entire plasma membrane at that stage. Inhibitor and cytological studies demonstrate that microfilaments and microtubules are responsible for early nuclear movement and migration toward the cortex (Foe and Alberts, 1983; Hatanaka and Okada, 1991; Baker et al., 1993). The cytoskeletal elements undergo rearrangements during the syncytial blastoderm stage (Karr and Alberts, 1986; Kellogg et al., 1988). During interphase, F-actin forms a cap above a pair of centrosomes that lie on the apical side of each nucleus. Starting from prophase, each of the pair of centrosomes separates and migrates to opposite sides of the nucleus to assemble a mitotic spindle, while the actin cap enlarges and spreads into pseudocleav-

C.X. Zhang and M.P. Lee share first authorship.

Address all correspondence to Tao-shih Hsieh, Department of Biochemistry, Duke University Medical Center, Durham, NC 27710. Tel.: (919) 684-6501. Fax: (919) 684-8885. e-mail: hsieh@bchm.biochem.duke.edu.

M.P. Lee's present address is Department of Medicine, Johns Hopkins University School of Medicine, 1064 Ross, 720 Rutland Ave., Baltimore, MD 21205.

age furrows, the transient membrane invaginations surrounding each spindle. In anaphase, F-actin undergoes a recapping process above each tubulin aster and stays in the caps throughout telophase. The actin-based microfilament networks seem to be important for the separation of the adjacent mitotic apparati, since disruptions in actin organization would lead to centrosome clumping and defective spindles (Callaini et al., 1992; Postner et al., 1992; Sullivan et al., 1990, 1993). Soon after cycle 14 begins, microtubules grow from the centrosomes to surround each elongating nucleus, and actin filaments form a membrane-associated hexagonal array that invaginates, passing the bottom of each nucleus, and then closes off to form cells. The integrity of the cytoskeleton is shown to be required for mitosis and cellularization in the early embryo. Failure of proper cytoskeletal organization leads to abnormal nuclear morphology, such as nondisjunction of chromosomes and nuclear fusion (Sullivan et al., 1993). Although cytoskeletal behavior in early cycles has been extensively studied and well characterized, the molecular mechanism remains unknown. A key step toward understanding the molecular mechanism is to define the cytoskeletal components in biochemical detail. A group of actin-binding proteins from *Drosophila* embryos has been isolated by F-actin affinity chromatography (Miller et al., 1989). Most of them (>90%) colocalize with actin at some point during early development. Both myosin VI and annilin are identified from such analysis, and they seem to play important roles in organizing the embryonic cytoskeleton (Field and Alberts, 1995; Mermall and Miller, 1995). Genetic approaches have also been applied in identifying components in embryonic cytoskeleton, either by analyzing the maternal effect mutants (Postner et al., 1992; Sullivan et al., 1990, 1993) or by reverse genetics (Karess et al., 1991).

We have recently generated a number of female sterile mutants, and one of them is a novel mutant that arrests the embryonic development during the transition from syncytial to cellular blastoderm. The cleavage furrows in the mutant embryos are grossly disrupted, suggesting this maternal effect gene is involved in the formation of embryonic cytoskeleton. According to the mutant phenotype, we name the gene affected in this mutant as discontinuous actin hexagon (*dah*). We have cloned and sequenced this gene, and its amino acid sequence shares limited homology with a family of cytoskeletal proteins, dystrophin, and apodystrophins. We have also generated specific antibody to monitor the expression and distribution of this protein. The maximal expression is at the syncytial/cellular blastoderm, thus coinciding with the genetic function of this protein. The immunofluorescence experiments have localized this protein in pseudocleavage and cleavage furrows, suggesting a functional role of this protein in the organization of early embryonic cytoskeleton.

## Materials and Methods

### Isolation of Female Sterile Mutants

*Drosophila* strain *438* (Bloomington Stock Center, Bloomington, IN) contains a P-element insertion at 13C1 in the X chromosome (de Cicco and Spradling, 1984). We have screened for mutants generated by imprecise excision events after remobilizing the P-element in *438* flies using a genomic source of transposase (Lee et al., 1993). Among the mutants characterized after this genetic screen, a lethal complementation group including *77*, *111*, *112*, and *113* was isolated. Their mutations were due to a deficiency in *top1* gene, which encodes DNA topoisomerase I, and could be completely rescued by an ectopic copy of *top1* introduced through germline transformation (Lee et al., 1993 ; see also Fig. 1 *A*). We have also isolated a female sterile group including alleles of *30* and *36*, which is in a different genetic complementation group from *top1* lethals. All of these mutants were subjected to the rescue tests by various transgenes containing genomic segments covering *top1* and neighboring sequences. Complementation tests of *top1* lethals were carried out as described before (Lee et al., 1993). For the female sterile mutants, genetic crosses were carried out to obtain homozygous female steriles of *fs(1)30* or *36* with either a balancer second chromosome *CyO*/+ or a second chromosome containing an ectopic copy of transgene, like p[*DSR*]/+ or p[*top1*]/+. These females were then mated with wild-type males. Only females with p[*DSR*] transgenes could produce progeny. For a given transgene construct, we have obtained several independent transformant lines, and the genetic rescue data were all consistent among each other.

### Molecular Genetics of dah

The molecular cloning of the genomic and cDNA sequences, nucleotide sequence analysis, PCR amplification, Northern blots, and immunoblots were carried out according to standard procedures (Sambrook et al., 1989). cDNA clones were isolated from an embryonic cDNA library (Nolan et al., 1986), and the cloning of genomic DNA in *top1/dah* locus was described earlier (Lee et al., 1993). The construction of the P-element transformation vector containing *top1/dah* genomic sequences, germline transformation, and screening/maintenance of the transformant lines followed the established protocols (Robertson et al., 1988; see also Roberts, 1986 ; with details specified in our earlier work, Lee et al., 1993). Database search and homology comparison were performed with Wisconsin Sequence Analysis Package (Genetics Computer Group, Madison, WI). The homology was first identified by BLAST search and subsequently analyzed by BestFit and GAP. Prediction of coiled-coil structure was made with software provided by Dr. Alex Knight (Whitehead Institute, Cambridge, MA) using a published algorithm (Lupas et al., 1991; Knight, 1994).

### Immunoblot Analysis

The cDNA encoding full-length *dah* protein was cloned into a T7 expression vector pET3a (Studier et al., 1990) for expression in bacteria. The over-produced protein represented ~30% of total bacterial protein. The recombinant *dah* protein was purified by differential centrifugation and SDS-PAGE. The purified *dah* was used to raise antibody in rabbit and coupled covalently to activated agarose beads (Reacti-Gel; Pierce Chemical Co., Rockford, IL). Rabbit antibody was affinity purified from *dah*-agarose column and showed exquisite specificity for a 71-kD protein in the *Drosophila* early embryo extracts. Embryonic extracts from different developmental stages were prepared as described earlier (Lee et al., 1993). Total protein of 100 μg from each sample was run on an 8% SDS polyacrylamide gel and electroblotted to a nitrocellulose filter. Immunodetection was carried out with a chemiluminescent ECL kit (Amersham Corp., Arlington Heights, IL) according to the manufacturer's protocol.

### Immunofluorescent Staining of Whole-Mount Embryos

Embryos from homozygous female sterile mutant or wild-type mothers were collected on grape juice plates at 25°C for a period of 30 min. They were staged by incubating in a humid chamber, and embryos of appropriate age were collected and washed with 0.7% NaCl and 0.05% Triton X-100. After dechorionation with 50% Clorox for 2 min, embryos were fixed in a 1:1 mixture of heptane and 8% formaldehyde for 20 min. For microtubule staining, taxol was added to the fixative following a protocol developed by Karr and Alberts (1986). While this fixation procedure may introduce artefactual microtubule staining at the centrosomal region (Kellogg et al., 1988), we have observed a less dramatic effect on centrosome structure (see, for example, Fig. 4, *A* and *B*). Furthermore, we are using microtubule staining, in conjunction with nuclear morphology, primarily for determining the phase of nuclear cycle in these embryos. The heptane layer containing the embryos was removed and mixed with methanol by vigorous shaking to rupture the vitelline membrane. For phalloidin staining of the F-actin, hand-peeling was used for vitelline removal. After rehydration and washing in PBS, embryos were incubated in 0.1% saponin and 1% normal goat serum in PBS for 30 min, and then overnight

with primary antibodies. The rabbit antibody against *dah* protein was affinity purified and then preadsorbed with *dah*$^-$ embryos. For staining microtubules, monoclonal mouse anti-α-tubulin antibody (T9026; Sigma Chemical Co., St. Louis, MO) was used. The embryos were then washed with PBS and incubated with Cy3-conjugated goat anti-rabbit or anti-mouse secondary antibody (Jackson ImmunoResearch Laboratories, West Grove, PA) for 1 h in the dark. After washing in PBS, they were incubated with fluorescein-conjugated phalloidin (Molecular Probes, Inc., Eugene, OR) and 4′,6-diamidino-2-phenylindole (DAPI)[1] (Sigma Chemical Co.) for 20 min in the dark. After final washing in PBS, the embryos were mounted in 90% glycerol, 0.1 M Tris-HCl, pH 8.0, and 0.5% wt/vol *n*-propyl gallate.

For nuclear morphology studies of the wild-type and *dah*$^-$ embryos, epifluorescence from DAPI staining was photographed with a microscope (Laborlux; E. Leitz, Inc., Rockleigh, NJ) on TMAX 400 film (Eastman-Kodak Co., Rochester, NY). The nuclear cycle was determined based on nuclear density counts. The laser scanning confocal images were collected using a fluorescence microscope (Axiovert; Carl Zeiss, Inc., Thornwood, NY) equipped with a ×40/1.30 Plan-Neofluar lens. The triple-stained embryos were first staged by epifluorescence from DAPI to monitor the nuclear morphology before it was switched to the confocal mode.

## Results

### Isolation of a New Female Sterile Mutant with an Early Embryonic Lethal Phenotype

We have previously used P-element transposon-mediated mutagenesis to generate lethals deficient in the topoisomerase I gene, which is located at 13C1 on the X chromosome (Lee et al., 1993; see also Fig. 1 *A*). We have isolated additional female sterile and lethal mutants and have carried out genetic crosses to group them into different complementation groups. All the lethals form one complementation group, which corresponds to deficiencies in *top1*. One of the female sterile complementation groups, which includes two alleles, *fs(1)30* and *fs(1)36*, appears to affect the early embryonic development and has been further characterized. While male flies are not affected by these mutations, females with either homozygous or heterozygous mutations in these two alleles develop normally and deposit eggs with normal morphology. However, these embryos fail to develop into the gastrulation stage. Further analysis indicates that there are extensive disruptions in the actin hexagonal arrays (see later sections in Results), and therefore, these mutants are named *dah* (discontinuous actin hexagon). These female steriles are clearly in a different complementation group than *top1* lethals, since the heterozygous fly like *fs(1) dah*$^{30}$/*l(1)top1*$^{77}$ is neither lethal nor sterile. To locate *dah* that is affected in these female steriles, we have generated germline transformants with transgenes of DNA segments in and around the *top1* locus (Fig. 1 *A*). A transgene of DNA segment downstream from the *top1* gene, p[*DSR*], can efficiently rescue the female sterile mutants of *fs(1) dah*$^{30}$ and *fs(1)dah*$^{36}$, but not the *top1* lethals. Conversely, a DNA segment covering *top1*, p[*top1*], can rescue *top1* lethals but not the female steriles. It is therefore likely that *dah*, which is responsible for the female sterile phenotype in *fs(1)dah*$^{30/36}$, is located in p[*DSR*].

To further analyze *dah*, we have isolated the gene covered in p[*DSR*]. Initial Northern experiments showed that using the 2.2-kb BamHI fragment in p[*DSR*] (Fig. 1 *A*) as a probe, a single transcript of 2.3 kb was detected in the early embryonic RNA preparation (data not shown). Using this BamHI fragment as the probe to screen an embryonic cDNA library, we have isolated several cDNA clones, all of which contain the same 3′ DNA sequence plus a poly A tail. The longest cDNA clone contains an insert of ~2.3 kb, suggesting that it is a nearly full-length cDNA clone. Sequence analysis of this cDNA and its comparison with the genomic DNA sequence reveal that it is generated from six exons with an open reading frame of 649 amino acid residues (Figs. 1 *B* and 2 *A*). The sequence at the initiating AUG agrees with the consensus of *Dro-*

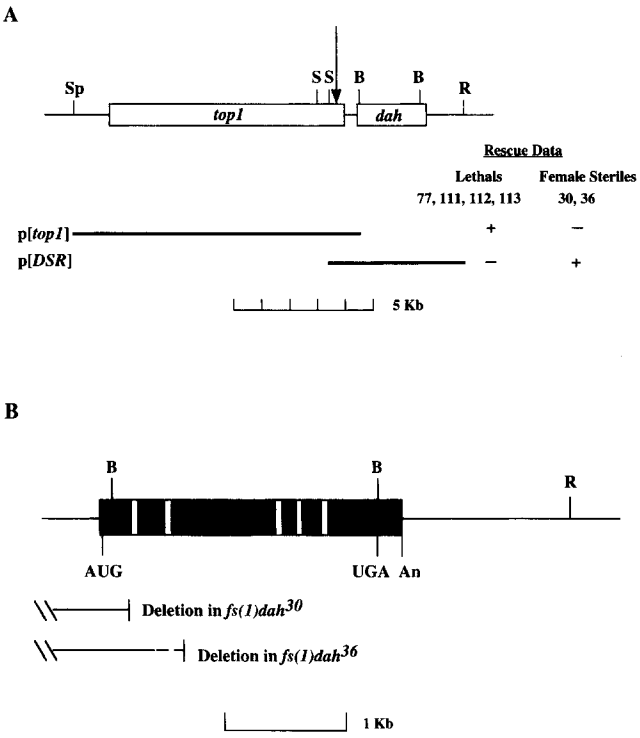


*Figure 1.* (*A*) Genetic complementation of lethal and female sterile mutants by an ectopic copy of genomic DNA fragment. Molecular map of the *top1* and *dah* region is indicated. The restriction sites of SpeI (*Sp*), SalI (*S*), BamHI (*B*), and EcoRI (*R*) are shown. The arrow indicates the insertion site of P-element in fly strain *438*, which was used in our mutagenesis experiment. We screened for the mutants generated by imprecise excision events associated with remobilized P-element. Shown here are six mutants that have been placed into two complementation groups. Four lethal mutants, *77*, *111*, *112*, and *113*, were rescued genetically by an ectopic copy of the *top1* gene, p[*top1*]. Two female sterile mutants, *30* and *36*, were rescued genetically by an ectopic copy of the *dah* gene, p[*DSR*]. The genetic rescue was performed with a transgenic second or third chromosome that was generated by introducing an ectopic copy of genomic DNA fragment, indicated as horizontal lines here, using P-element germline transformation. (*B*) Genomic structure of the *dah* gene. The exons are shown as filled boxes, and the introns are shown as open boxes. The restriction sites of BamHI and EcoRI are indicated as *B* and *R*, respectively. Translational start codon, AUG, and stop codon, UGA, are indicated. *An*, poly A addition site. Extents of deletions in the *dah* gene for two null mutants, *fs(1)dah*$^{30}$ and *fs(1)dah*$^{36}$, are demarcated as horizontal lines. The broken line at the end indicates the range of uncertainty in the deletion end point.

1. *Abbreviation used in this paper*: DAPI, 4′, 6-diamidino-2-phenylindole.

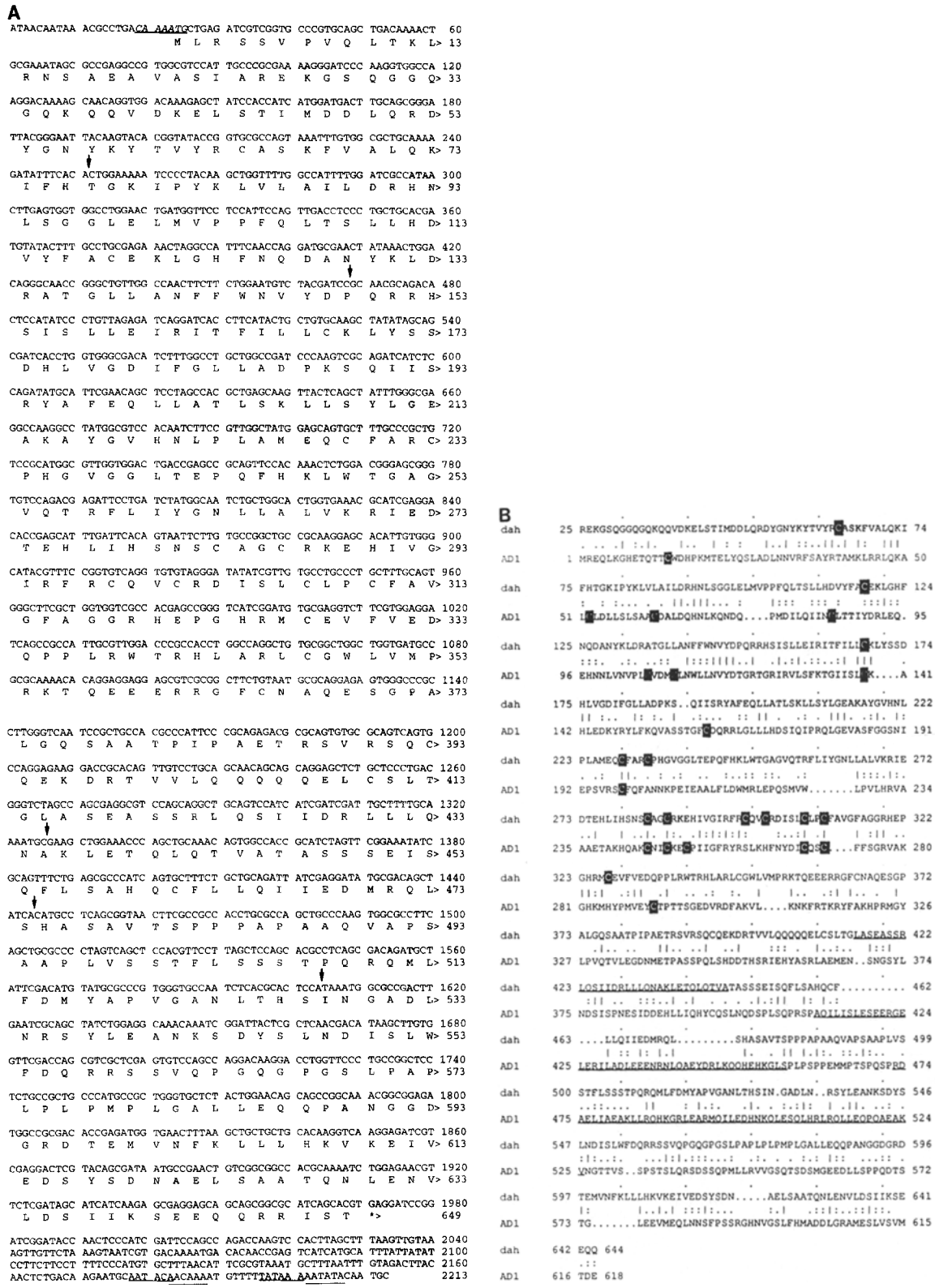


*Figure 2.* (*A*) Sequence of the *dah* cDNA and the encoded protein. The cDNA sequence of the *dah* gene and its translation are shown. The *Drosophila* consensus translational start is underlined and italicized. Arrows mark five exon-intron junctions, and underlined sequences toward the 3′ end identify the poly A cleavage/addition consensus sequence with single nucleotide substitutions. These sequence data are available from EMBL/GenBank/DDBJ under accession number U43786. (*B*) Sequence homology between the *dah* protein and apodystrophin-1. The sequence alignment shown is based on BestFit from GCG package, and identical alignment can be produced with GAP. Lines between two sequences mark identical residues, while colons and dots indicate residues with more or less similarities, respectively. Cysteines in cysteine-rich domain of apodystrophin-1 and corresponding region of *dah* are highlighted. Coil-coiled predictions based on Lupus algorithm are underlined.

*sophila* translational start (Cavener, 1987), and all the exon/intron junctions are consistent with the published consensus sequences (Mount et al., 1992). While there is no poly A cleavage/addition consensus sequence (AAUAAA) present near the 3′ end, there are four related sequences with single-nucleotide substitutions (Fig. 2 *A*; see also Sheets et al., 1990). We have physically mapped the mutations in *fs(1)dah*$^{30/36}$ in *dah* locus. *fs(1)dah*$^{30}$ contains a deletion, and its junctions are determined by PCR-coupled sequence analysis. It involves a deletion of 2.0-kb sequence with one deletion end point in *top1*, thereby removing 1.36 kb of 3′ untranslated region of *top1*. The other deletion end point is close to the junction of exon 1 and intron 1, removing the 5′ end of the gene, including the initiating AUG and 75 amino-terminal residues (Fig. 1 *B*). *fs(1)dah*$^{36}$ also contains a deletion, the exact end points of which are not determined. Genomic Southern experiments suggest that the deletion removes up to intron 2 and possibly exon 3 (Fig. 1 *B*). Therefore, both mutations are null and are consistent with their phenotype being recessive.

### *The Sequence of dah Protein Exhibits Limited but Significant Homology to Mammalian Apodystrophins*

The cytogenetic location and phenotype of *dah* indicate that they are novel mutants in *Drosophila.* Sequence searches with both genomic DNA sequences and the predicted open reading frame do not recover any entry in the *Drosophila* database. However, BLAST search of the GenBank database identifies homology between the *dah* protein and a family of proteins related to the COOH-terminal domains of dystrophin. Dystrophin is a multidomain protein of 427 kD and plays a critical role in the linkage of cytoskeleton to extracellular matrix in muscle cells (for review see Ahn and Kunkel, 1993; Blake et al., 1994). The $NH_2$-terminal domain is homologous to α-actinin, and the central domain consists of β-spectrin repeats (Koenig et al., 1988). The carboxyl terminus of dystrophin is characterized by a cysteine-rich region followed by a coiled-coil domain (Blake et al., 1995). Through the use of different promoters and RNA processing, there are a few smaller proteins expressing the carboxyl domains of dystrophin, including apodystrophin-1 (Dp71), apodystrophin-2, and apodystrophin-3 (Ahn and Kunkel, 1993; Blake et al., 1994). In addition, there is an 87-kD postsynaptic protein from the electric eel, which also displays modest homology (25% identity) with this region of dystrophin (Wagner et al., 1993).

The alignment between *dah* protein and apodystrophin-1 (or the carboxyl-terminal domains of dystrophin) shows sequence matches throughout these molecules (Fig. 2 *B*). There are 20% identities and 42% similarities in this homology alignment. By comparing the alignment of a randomized sequence pool generated from *dah* sequence, the homology score between *dah* protein and apodystrophin-1 is better than the mean of the randomized pool by more than eight standard deviations, thus suggesting that the limited homology between *dah* and apodystrophins is statistically significant. In the cysteine-rich region, corresponding to the amino-terminal domain of *dah*/apodystrophin, six of the cysteines are conserved and four of them are replaced by histidines or homologous substitutions (Fig. 2 *B*). After this domain, both proteins show a propensity for forming coiled-coil structure using an algorithm originated from Lupus et al. (1991). However, the exact locations of coiled-coil structures are not aligned between *dah* and apodystrophin (Fig. 2 *B*).

### *Embryos from dah Mutant Females Exhibit Extensive Nuclear Fusion Starting from Cycle 13 Anaphase*

Our initial results showed that embryos from *dah*$^-$ mothers could not enter gastrulation stages. To further analyze their cytological defects, we have examined the nuclear morphology of developing embryos collected between 0–3 h after oviposition. Since both *fs(1)dah*$^{30}$ and *dah*$^{36}$ remove 3′ untranslated sequence in *top1*, we used the transgenic fly strains of these mutants containing p[*top1*] to eliminate the potential effects from any variations of *top1* expression in *dah* mutants. However, for the mutants with or without the p[*top1*] transgene, our observations with the embryos are, in general, consistent with each other. Embryos from mutant mothers can develop more or less normally up to nuclear cycle 13 (data not shown). In the anaphase and telophase of cycle 13, right before cellularization started, the segregating nuclei in a mutant embryo do not have regular spacings any more (Fig. 3 *C*). These should be compared with clearly spaced nuclei at the same stage in a wild-type embryo (Fig. 3 *A*). At a higher magnification, the mutant embryo frequently contains closely packed pairs of daughter chromosomes that run parallel to each other, and neighboring chromosomes are in close contact (Fig. 3 *D*; compare with wild type in Fig. 3 *B*). During the interphase of nuclear cycle 14, there is extensive nuclear fusion over the entire surface (Fig. 3 *G*; compare with wild type in Fig. 3 *E*). Shown in higher magnification, the nuclear morphology of the mutant embryos is deteriorated by fusion events (mutant vs wild type in Fig. 3, *H* and *F*). These embryos arrest their development at this stage and never enter gastrulation. While *dah* function is not critical for the axial and cortical nuclear migration during early embryonic stages, it is needed for the blastoderm stages, a function consistent with it being a maternal effect gene.

### *Abnormal Nuclear Morphology in dah Mutant Embryos Is Correlated with Cytoskeletal Structure Defects*

Since cytoskeletal structure in early embryos plays a critical role in nuclear migration and divisions (for review see Schejter and Wieschaus, 1993; Miller and Kiehart, 1995), it is possible that the nuclear morphology defects in *dah*$^-$ mutants are correlated with defective cytoskeletal structure in the blastoderm stages. We have monitored the microtubule and F-actin structure in the mutant embryos, and apparent defects have been found in pseudocleavage furrows. One such example is shown for an embryo in the metaphase of cycle 12 (Fig. 4 *B* vs 4 *A*). Actin filaments of this mutant embryo show interruptions and discontinuities, especially at vertices where furrows intersect. However, most mitotic spindles appear normal, surrounded by a discontinuous actin network. The defects seem to be restricted to the pseudocleavage furrows because actin caps of the next cycle (cycle 13) form normally at the interphase (compare Fig. 4 *D* with 4 *C*). Similar observations

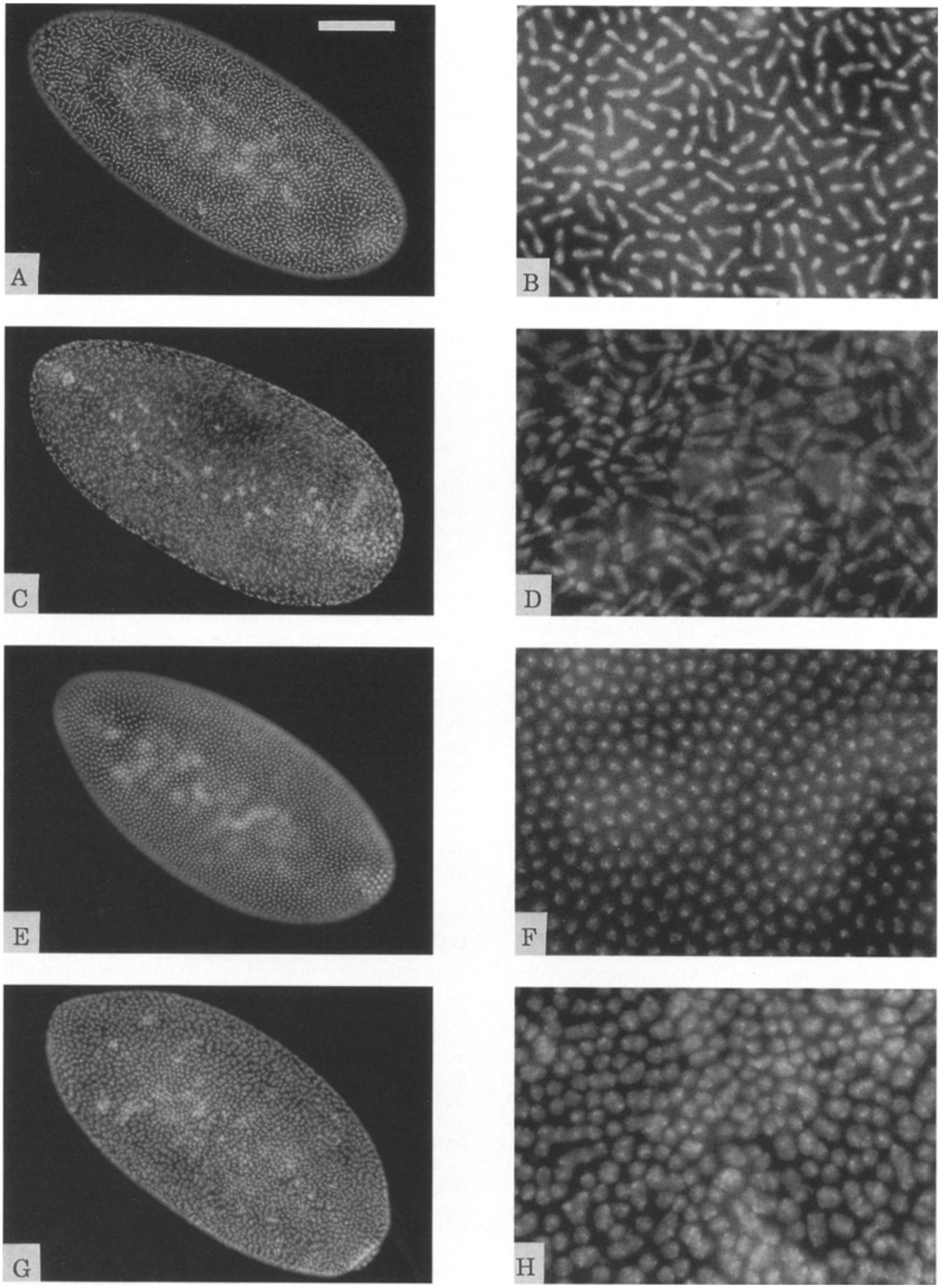
A
B
C
D
E
F
G
H

are also made in mutant embryos between cycles 11 and 13 in the syncytial blastoderm. The normal function of *dah* may be to stabilize the specialized cytoskeletal structure in these transient furrows. Absence of *dah* in null mutants results in disruptions of the furrows, especially at the intersecting points where stresses are expected to be the greatest. The furrow defect eventually leads to apparent nuclei fusion at the end of cycle 13. Since the nuclear density at cycle 13 is higher than at previous cycles, there is an increased probability of nuclear collisions without any stable physical barriers.

In addition to the defects in pseudocleavage furrows, cleavage furrows during cellularization are also disrupted in the mutant. For normal embryos at the cellularization stage, invaginating furrows form interconnected hexagons, each of which encloses a tubulin dome (Fig. 4, *E* and *G*). In marked contrast, *dah*$^-$ embryos have extensive disruptions in microfilament and microtubule structures (Fig. 4, *F* and *H*). The regularity and continuity of actin network are totally missing. Related to this observation, many furrows fail to invaginate properly (Fig. 4 *H*). The abnormal microtubule structure appears to correlate with nuclear defects: different sizes of tubulin domes cap different numbers of nuclei that have been fused together (data not shown). Therefore, the nuclear morphology defect observed in the cycle 14 interphase, as described earlier (see Fig. 3, *G* and *H*), is also related to the disruptions of cytoskeletal structure at cleavage furrows.

### *Dah Protein Is Expressed Only in the Early Embryonic Stages*

The cytogenetic data suggest that *dah* gene product is critical for embryonic development during blastodermal stages. To monitor the expression of *dah* protein during *Drosophila* embryogenesis and to localize its distribution, we have expressed *dah* in bacteria and used it to generate polyclonal antibody. The isolated 71-kD recombinant *dah* protein also served as a ligand to purify rabbit antibody by affinity chromatography. The specificity of *dah* antibody was examined by immunoblots of embryo extracts. Protein extracts were prepared from the following three embryo samples: wild type, *dah* mutant, and *dah* mutant with p[*DSR*] to rescue *dah* phenotype. Identical amounts of protein were loaded on an SDS polyacrylamide gel (Coomassie-stained portion; Fig. 4 *A*). From the immunoblots of the same gel, *dah* antibody specifically detects a single band with a size of 71 kD in the wild-type embryos (Fig. 5 *B*, lane *6*). This signal is missing in *dah*$^-$ embryos (Fig. 5 *B*, lane *7*) and restored in embryos from *dah*$^-$ mother with p[*DSR*] transgene (Fig. 5 *B*, lane *8*). When other proteins, DNA topoisomerases I and II, are examined in the same set of samples, all three samples yield comparable amounts of signal (Fig. 5, *C* and *D*). In addition to demonstrating the specificity of *dah* antibody, these results also confirm that the defects in *dah*$^-$ embryos are caused by the absence of *dah* expression.

We have monitored *dah* expression during various developmental stages to further understand the function of *dah* protein during *Drosophila* development. Both the Northern analysis and immunoblots (Fig. 6, *A* and *B*) show that *dah* expression is primarily in the embryos with ages spanning 0–6 h. While *dah* protein expression is only detected in the embryos at the early stages of development, *dah* message is observed both in early embryos and adult flies (Fig. 6, lanes *9* in *A* and *B*). The adult expression of *dah* message is primarily limited to the ovaries (data not shown), a result consistent with maternal function of *dah* gene product. However, no protein expression could be detected in ovaries (data not shown). To further define the expression pattern of *dah* protein during early embryonic development, we prepared the extracts from embryos that were staged hourly between 0 and 6 h. The expressions of *dah* protein in these embryos were analyzed by quantifying the immunoblot data (Fig. 6 *C*). The maximal expression is in the embryos of 2–3-h-old, and the signal rapidly declines beyond this point. This period of embryonic development corresponds to the transition between syncytial blastoderm (cycle 13) and cellularization in cycle 14 (for review see Foe et al., 1993). We have also monitored the stage of development in our embryo collection by the nuclear staining with DAPI, and they are within these nuclear cycles. The cytological studies of the *dah*$^-$ mutants indicate that *dah* gene is essential for embryonic development from cycle 13 to cycle 14. The maximal expression of *dah* protein therefore appears to coincide with the period when *dah* gene is critically required.

### *Localization of dah Protein in the Pseudocleavage and Cleavage Furrows*

The mutant phenotype studies suggest that *dah* may be involved in setting up pseudocleavage furrows in the syncytial blastoderm and cleavage furrows in the cellular blastoderm. To address this question, we have localized *dah* protein and a known cytoskeletal protein, F-actin, during the early development. Colocalization of these two proteins will give rise to yellow/orange signals in the overlays of the immunofluorescence images shown in Fig. 7.

***Preblastoderm.*** Before cycle 10, all nuclear divisions occur in the interior of the embryos. In these preblastoderm stages, a number of cytoskeletal components including actin, tubulin, $\alpha/\beta_H$ spectrin isoforms, and myosin colocalize in a cortical layer underneath the cytoplasmic membrane of the embryos (Warn et al., 1984; Karr and Alberts, 1986; Pesacreta et al., 1989; Young et al., 1991; Thomas and Kiehart, 1994). *Dah* protein signal, also found in the cortex (Fig. 7 *A*), colocalizes with actin. Since *dah*$^-$ embryos show no apparent abnormalities at this stage and can de-

*Figure 3.* Abnormal nuclear morphology in embryos derived from homozygous *dah*$^-$ mothers. Embryos were stained with DAPI to reveal nuclear morphology. Mutant embryos (*C*, *D*, *G*, and *H*) are compared with those of wild type (*A*, *B*, *E*, and *F*). (*Left*) Structures of whole embryos; (*right*) magnified fivefold to reveal nuclear morphologies. The upper four panels (*A–D*) show embryos in the anaphase of cycle 13. The irregular nuclear distribution and local fusions of neighboring nuclei are observed in a *dah*$^-$ embryo. The bottom four panels (*E–H*) show embryos in cellularization. Nuclear fusions in a mutant embryo are extended over the entire surface at this stage. Bars: (*A*, *C*, *E*, and *G*) 100 μm; (*B*, *D*, *F*, and *H*) 20 μm.

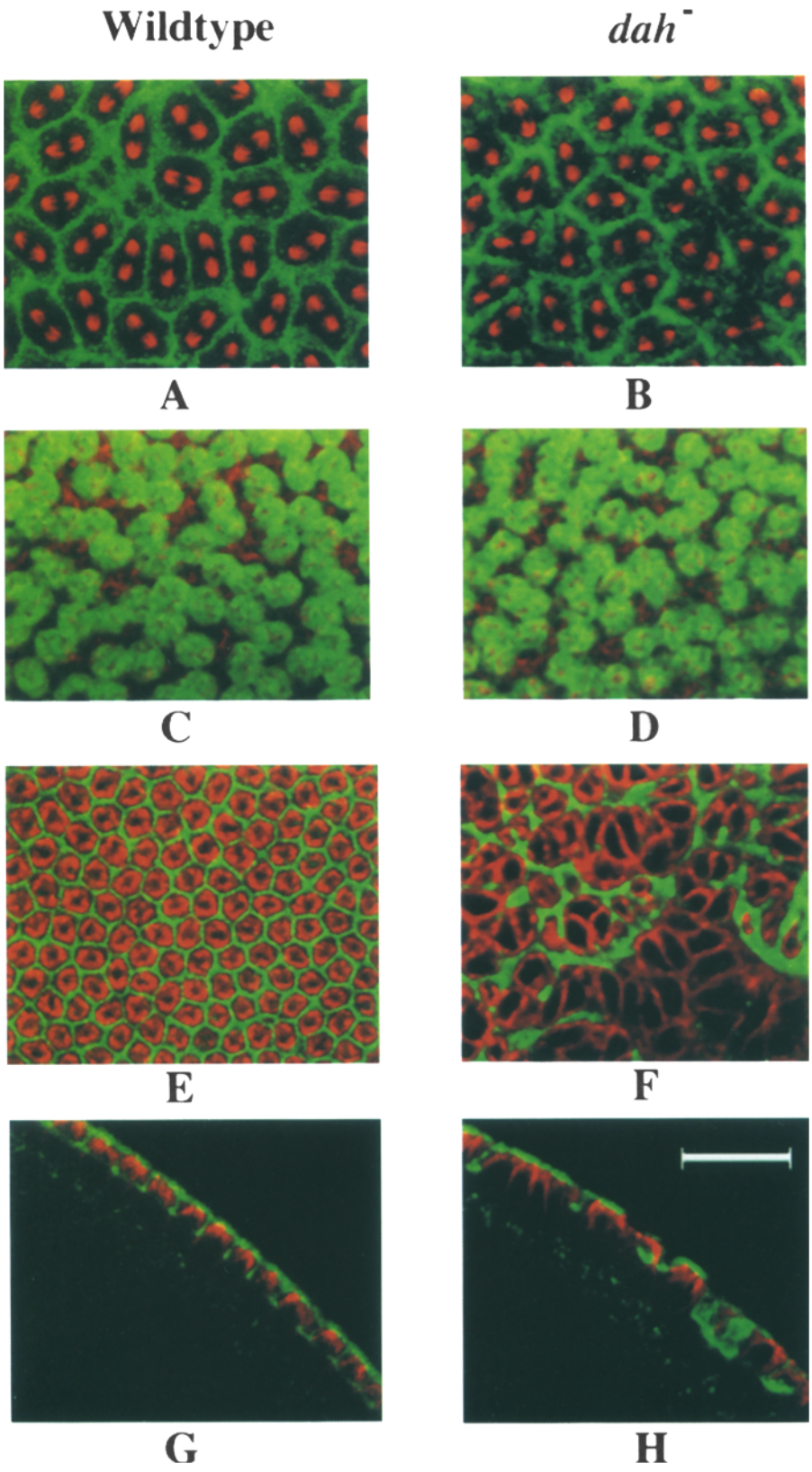


*Figure 4.* Defects in cytoskeletal structure. Mutant embryos in blastoderm stages (*right panels*) are compared with those of wild type (*left panels*). Phalloidin conjugated with fluorescein (*green channel*) was used to reveal microfilament structures, and antibody conjugated with Cy3 (*red channel*) was used to reveal microtubule structures. In embryos at cycle 12 metaphase (*A* and *B*), local disruptions at the vertices of the microfilaments are observed in the mutant embryo. However, actin caps form normally in the interphase of next cycle (*C* and *D*). Microfilament and microtubule structures are both disrupted during cellularization (*E–H*). *E* and *F* show the en face views of a wild-type and a mutant embryo, respectively. *G* and *H* show the sagittal views of same embryos as in *E* and *F*. Bar, 25 μm.

velop into blastoderm, *dah* is not likely to play an important role in the early nuclear divisions and migration. The cortical distribution of *dah* in the preblastoderm is probably for storage and for the preparation of the arrival of nuclei at the cortex during the blastoderm stage.

***Syncytial Blastoderm.*** For embryos at this stage (cycles 10–13), nuclei are not separated by any cellular membrane; instead, they are partitioned by specialized cytoskeletal structures, pseudocleavage furrows. Many cytoskeletal components including actin and myosin are concentrated

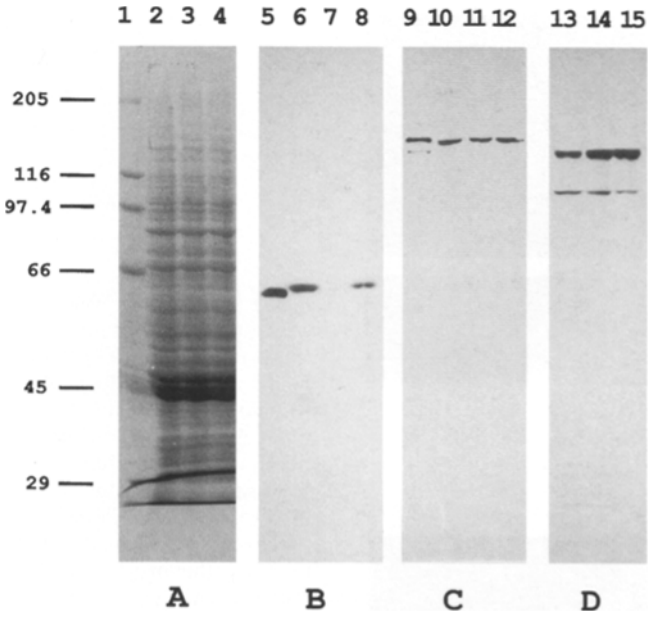


*Figure 5.* Protein expressions in wild-type and mutant embryos. (*A*) Coomassie staining. Lane *1* was loaded with molecular weight markers. Lanes *2*, *3*, and *4* were loaded with crude extracts of embryos derived from wild type, *dah*$^-$, and *dah*$^-$ with p[*DSR*] transgene mothers, respectively, in comparable total protein amounts (100 μg). (*B–D*) Immunoblot analysis of *dah*, topoisomerase II, and topoisomerase I proteins. Three sets of embryo samples were loaded on the same gel for Western blot. They were transfered to nitrocellulose and probed with antibodies specific for *dah*, topoisomerase II, and topoisomerase I in *B–D*, respectively. Lanes *5* and *9* were purified *dah* and topoisomerase II proteins expressed in *Escherichia coli.* Lanes *6–8*, *10–12*, and *13–15* were identical sets as lanes *2–4. Dah* is missing in *dah*$^-$ embryos only, while topoisomerase II and topoisomerase I expression levels in all three strains are comparable. The minor, lower bands in the topoisomerase I blot are likely due to proteolytic degradation in the crude extract.

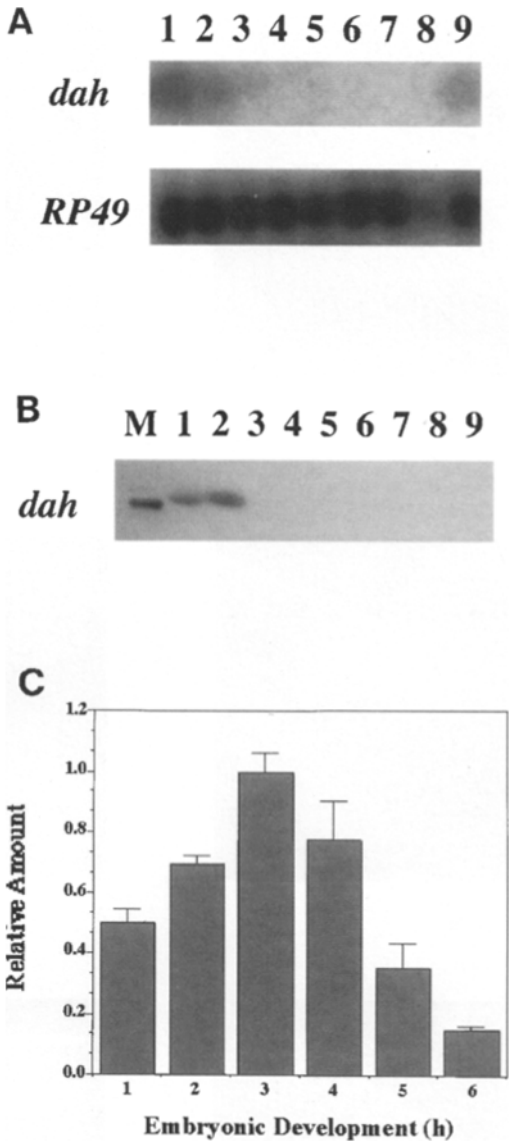


*Figure 6.* Developmental regulation of the *dah* gene expression. (*A*) Developmental Northern analysis. Total RNA was extracted from different developmental stages: 0–2-, 2–6-, 6–12-, and 12–20-h embryos; larvae of different instar stages at I1, I2, and I3; pupa; and adults (lanes *1–9*). Identical amounts (5 μg) of total RNA were loaded in each lane and processed for blot/hybridization probed by either *dah* (*upper panel*) or *RP49* as loading controls (*lower panel*). The *dah* probe was derived from 1.9-kb BamHI cDNA fragment in *dah* (see Fig. 1 *B*). The *dah* transcript can be detected in 0–2-h and 2–6-h embryos and adult collections. The amount of mRNA in the pupal sample was lower by ~50%. However, an overexposure of *dah*-probed blot failed to reveal any signal in pupal sample. (*B*) Developmental Western analysis. Total proteins were extracted from the same developmental stages as above. Recombinant *dah* protein isolated from *E. coli* was loaded in lane *M* to serve as a marker. Around 100 μg of total protein was loaded in each lane. *Dah* expression is detected only in 0–2- and 2–6-h embryos. (*C*) Quantitation of the *dah* protein expression. The relative amounts of *dah* expression during the first 6 h of embryogenesis were determined by densitometry of immunoblots. The error bars depict SD from three independent experiments.

there. In the pseudocleavage furrows, *dah* protein colocalizes with F-actin, based on both sagittal and surface images (Fig. 7 *B*, *upper* and *lower panels*). However, there is a significant difference in the spatial distribution of these two proteins as evidenced by the green staining on the surface and yellow/orange staining in the furrow regions. Actin is evenly distributed underneath the entire plasma membrane with invaginations to encircle the dividing pair of mitotic chromosomes (Karr and Alberts, 1986; see also Fig. 7 *B*). On the other hand, *dah* protein appears to be more concentrated in the pseudocleavage furrows, thus giving a more intense staining there (Fig. 7 *B*). During anaphase, actin retreats from the pseudocleavage furrows and redistributes as caps over each newly formed nucleus (Karr and Alberts, 1986). While *dah* protein also undergoes redistribution, a significant amount of *dah* still remains in the pseudocleavage furrows (data not shown). Furthermore, *dah* is concentrated in between the divided pair of nuclei, a position marked as the furrows for the next nuclear cycle. Initial experiments indicate that a fraction of *dah* is persistently distributed in the furrows throughout the nuclear cycles, strongly suggesting a critical role for *dah* in organizing these specialized cytoskeletal structures.

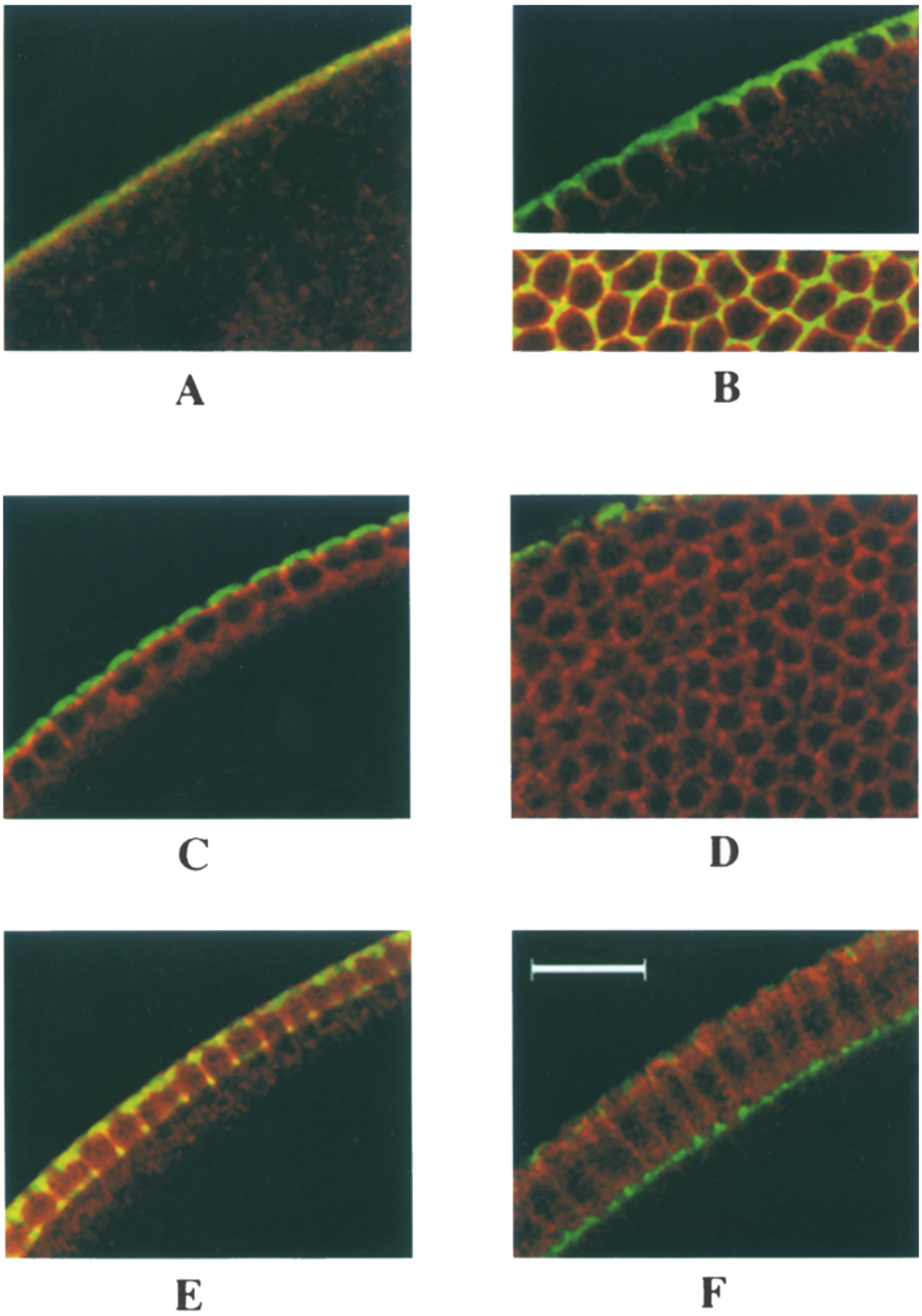


*Figure 7.* The *dah* protein localization in early embryos. Wild-type embryo was stained by indirect immunofluorescence with *dah* antibody, followed by Cy3-conjugated secondary antibody (*red*) and fluorescein-conjugated phalloidin (*green*) to reveal *dah* and F-actin, respectively. All images shown here are the overlays of red/green channels. (*A*) Sagittal view of a preblastoderm embryo in cycle 9, where *dah* colocalizes with F-actin in a cortical layer underneath plasma membrane. (*Upper* and *lower panels* in *B*) Sagittal and en face views, respectively, of the same embryo in cycle 13. *Dah* protein concentrates in the pseudocleavage furrows. (*C* and *D*) Sagittal and subsurface (at a focal plane 4 μm below the embryo surface) views, respectively, from the same embryo in early interphase of cycle 14, right before cellularization. Actin filaments are still in caps, while *dah* marks the future cleavage furrow positions. (*E*) Sagittal image of an embryo in the slow phase of cellularization. *Dah* is concentrated in membrane invaginations, but also distributed ahead of the furrow fronts. The membrane front catches up with *dah* distribution in fast phase of cellularization, when invaginating membrane passed the bottom of nuclei (*F*). Bar, 25 μm.

***Cellular Blastoderm.*** During the interphase of cycle 14, the membrane invaginates to form cleavage furrows around each of the ~6,000 cortical nuclei. Most of the components in the pseudocleavage furrows participate in the formation of the cleavage furrows in cycle 14 as well. At early interphase of cycle 14, before cellularization, F-actin forms caps, and *dah* protein concentrates at the edges of the actin caps (Fig. 7 *C*). In addition, *dah* marks presumptive, future cleavage furrows deep into the cytosol. This is evidenced by an image taken 4 μm below the embryo surface in which *dah* protein shows punctate staining in those presumptive furrows (Fig. 7 *D*). Actin remains in the caps and is not present in these furrow locations (Fig. 7 *D*). During the slow phase of cellularization, *dah* concentrates in cleavage furrows and also has similar punctate furrow staining ahead of the furrow canals that mark the invaginating membrane fronts (Fig. 7 *E*). Actin networks are mainly found in the membrane fronts at this stage (Fig. 7 *E*). When the fast phase of cellularization starts, *dah* signal is primarily in the cleavage furrows and not detected anywhere else (Fig. 7 *F*). It may be associated with the newly formed plasma membranes around each elongated nucleus. Actin filaments concentrate in the invaginating front of the furrow canals and in the basal constrictive rings

(Fig. 7 *F*). *Dah* protein signal remains after cellularization finishes, and eventually disappears before the stage of slow germ band extension (data not shown).

## Discussion

*Drosophila* early embryos provide a unique system to study the functions of the cytoskeleton in nuclear and cell division (Schejter and Wieschaus, 1993; Miller and Kiehart, 1995). The pseudocleavage furrows in the syncytial blastoderm, cleavage furrows during cellularization, and contractile rings in cytokinesis share some common cytoskeletal organization, although each has its distinct elements. All the components in the pseudocleavage furrows are endowed by the mother in the form of either RNA or protein. Cleavage furrows inherit and share most components from the pseudocleavage furrows, with the addition of three zygotic genes, *nullo*, *serendipity-α*, and *bottleneck* (Merrill et al., 1988; Wieschaus and Sweeton, 1988; for review see Schejter and Wieschaus, 1993). It has been proposed that the maternal genes set up the furrow structure initially, and these zygotic gene products modify and remodel the cytoskeleton for the specific roles during cellularization (Schejter et al., 1992; Postner and Wieschaus, 1994).

We have isolated a new maternal effect mutation and demonstrated its gene product to be essential for the development of blastoderm. The *dah* gene product is primarily stored in the form of RNA by the mother, and the maximal protein expression is during the transition from syncytial to cellular blastoderm. Cytogenetic data and immunolocalization experiments presented here show that *dah* protein is a critical component for both pseudocleavage furrows in the syncytial blastoderm and cleavage furrows during the cellularization process. Furthermore, *dah* protein is also present in the presumptive furrows ahead of invaginating fronts before the fast phase of cellularization. It is possible that *dah* plays a critical role in the initiation of the cleavage furrow development. Cytological analysis of several maternal effect mutants has shown that their gene products are involved in the proper formation of pseudocleavage furrows. These maternal mutations, including *sponge* (Postner et al., 1992), *dal* (Sullivan et al., 1990), *scrambled*, and *nuclear-fallout* (Sullivan et al., 1993), disrupt cytoskeletal structures in early embryos, resulting in abnormal nuclear morphology. Similar to the *dah* mutant, the *nuclear-fallout* mutant has disrupted both pseudocleavage and cleavage furrows, while *sponge*, *dal*, and *scrambled* have abnormal furrows in the syncytial blastoderm but form nearly normal cytoskeletal structure at the cellularization stage. It is possible that *sponge*, *dal*, and *scrambled* are distinct elements involved in pseudocleavage furrows, while *nuclear-fallout* and *dah* are involved in both furrow formations.

Sequence search has revealed homology between *dah* and the COOH terminus of dystrophin and apodystrophins. The COOH terminus of dystrophin is unique to a family of proteins, including dystrophin, dystrophin-related proteins, and apodystrophins. It is plausible that *dah* might share the same ancestral origin as the COOH terminus of dystrophin. The function of dystrophin is proposed to link the extracellular matrix through the membrane protein complex to the actin-based cytoskeleton, therefore stabilizing the sarcolemma structure under contractile stress. Both biochemical and cell biological experiments suggest the association of dystrophin with sarcolemma membrane in adult muscles is mediated through glycoprotein complexes (for review see Ahn and Kunkel, 1993; Ervasti and Campbell, 1993). The glycoprotein binding sites have been mapped to the COOH-terminal domains by biochemical analysis of calpain-treated dystrophin (Suzuki et al., 1992). Transgenic experiments with apodystrophin-1 (Dp71) demonstrate that the COOH-terminal domains of dystrophin can associate with sarcolemma membrane and organize the dystroglycan complex formation (Cox et al., 1994). An 87-kD protein isolated from the postsynaptic membrane of the electric organ of electric eel also shows modest homology with apodystrophin-1 (Wagner et al., 1993). This protein is a component of the cytoskeletal structure at the neuromuscular junctions. It may serve to cluster and stabilize nicotinic acetylcholine receptor (Butler et al., 1992; Wagner et al., 1993). While the homology between *dah* and the dystrophin COOH terminus is limited, *dah* is localized in a specialized cytoskeletal structure, and initial fractionation data suggest it is present in the membrane preparations (data not shown). Therefore, the biochemical basis of *dah* functions might share some features with dystrophin and the family of apodystrophins. It is possible that *dah* serves to organize and stabilize the cytoskeleton associated with embryonic cleavage furrows. Interestingly, in *dah* mutant embryos, disruptions of metaphase furrows often happen around the vertices. These are points where one would expect the mechanical stress generated by the dividing nuclei to be the greatest. Therefore, *dah* seems to be important for stabilizing the actin cytoskeleton under stress, a role also shared by dystrophin in skeletal muscles.

The $dah^-$ alleles we have isolated are null mutations. These *dah* mutants are phenotypically tight; no embryos from homozygous $dah^-$ mothers develop beyond cellular blastoderm. Our results demonstrate that *dah* is a component participating in the organization and maintenance of cortical furrows. While *dah* has an essential function in blastoderm development, it does not rule out other potential functions later in development. Missing these other functions may not affect the viability of the fly. However, our immunochemical data suggest that *dah* protein is not present at significant levels in any developmental stages other than early embryos, thus arguing against this possibility. *Dah* is also unlikely to be critically involved in the conventional cytokinetic contractile rings since pole cells can bud off in the mutant embryos (data not shown), and the homozygous $dah^-$ embryo from a mother with a heterozygous *dah* mutation can develop into an adult fly. Future analysis on the precise functions of *dah* in the cortical metaphase and cellularization furrows should provide insights into the organization and regulation of these specialized cytoskeletal structures.

We thank Prof. R. Fehon (Duke University) for sharing with us his protocols for immunofluorescence staining of whole-mount embryos.

This work is supported by a grant from the National Institutes of Health (GM29006).

Received for publication 2 April 1996 and in revised form 28 May 1996.

*References*


Ahn, A.H., and L.M. Kunkel. 1993. The structural and functional diversity of dystrophin. *Nat. Genet.* 3:283–291.

Baker, J., W.E. Theurkauf, and G. Schubiger. 1993. Dynamic changes in microtubule configuration correlate with nuclear migration in the preblastoderm *Drosophila* embryo. *J. Cell Biol.* 122:113–21.

Blake, D.J., J.M. Tinsley, and K.E. Davies. 1994. The emerging family of dystrophin-related proteins. *Trends Cell Biol.* 4:19–23.

Blake, D.J., J.M. Tinsley, K.E. Davies, A.E. Knight, S.J. Winder, and J. Kendrick-Jones. 1995. Coiled-coil regions in the carboxy-terminal domains of dystrophin and related proteins: potentials for protein-protein interactions. *Trends Biochem. Sci.* 20:133–135.

Butler, M.H., K. Douville, A.A. Murnane, N.R. Kramarcy, J.B. Cohen, R. Sealock, and S.C. Froehner. 1992. Association of the $M_r$ 58,000 postsynaptic protein of electric tissue with *Torpedo* dystrophin and the $M_r$ 87,000 postsynaptic protein. *J. Biol. Chem.* 267:6213–6218.

Callaini, G., R. Dallai, and M.G. Riparbelli. 1992. Cytochalasin induces spindle fusion in the syncytial blastoderm of the early *Drosophila* embryo. *Biol. Cell.* 74:249–254.

Cavener, D.R. 1987. Comparison of the consensus sequence flanking translational start sites in *Drosophila* and vertebrates. *Nucleic Acids Res.* 15:1353–1361.

Cox, G.A., Y. Sunada, K.P. Campbell, and J.S. Chamberlain. 1994. Dp71 can restore the dystrophin-associated glycoprotein complex in muscle but fails to prevent dystrophy. *Nat. Genet.* 8:333–339.

de Cicco, D.V., and A.C. Spradling. 1984. Localization of a cis-acting element responsible for the developmentally regulated amplification of *Drosophila* chorion genes. *Cell.* 38:45–54.

Ervasti, J.M., and K.P. Campbell. 1993. Dystrophin and the membrane skeleton. *Curr. Opin. Cell Biol.* 5:82–87.

Field, C.M., and B.M. Alberts. 1995. Anillin, a contractile ring protein that cycles from the nucleus to the cell cortex. *J. Cell Biol.* 131:165–178.

Foe, V.E., and B.M. Alberts. 1983. Studies of nuclear and cytoplasmic behavior during the five mitotic cycles that precede gastrulation in *Drosophila* embryogenesis. *J. Cell Sci.* 61:31–70.

Foe, V.E., G.M. Odell, and B.A. Edgar. 1993. Mitosis and morphogenesis in the Drosophila embryo: point and counterpoint. *In* The Development of *Drosophila melanogaster.* Vol. 1. M. Bate and A.M. Arias, editors. Cold Spring Harbor Laboratory, Cold Spring Harbor, NY. 149–300.

Fyrberg, E.A., and L.S. Goldstein. 1990. The *Drosophila* cytoskeleton. *Annu. Rev. Cell Biol. 6:559–596.*

Hatanaka, K., and M. Okada. 1991. Retarded nuclear migration in Drosophila embryos with aberrant F-actin reorganization caused by maternal mutations and by cytochalasin treatment. *Development (Camb.).* 111:909–920.

Karess, R.E., X.J. Chang, K.A. Edwards, S. Kulkarni, I. Aguilera, and D.P. Kiehart. 1991. The regulatory light chain of nonmuscle myosin is encoded by *spaghetti-squash*, a gene required for cytokinesis in *Drosophila. Cell.* 65: 1177–1189.

Karr, T.L., and B.M. Alberts. 1986. Organization of the cytoskeleton in early *Drosophila* embryos. *J. Cell Biol.* 102:1494–1509.

Kellogg, D.R., T.J. Mitchison, and B.M. Alberts. 1988. Behaviour of microtubules and actin filaments in living *Drosophila* embryos. *Development (Camb.).* 103:675–686.

Knight, A.E. 1994. The diversity of myosin-like proteins. Ph.D. dissertation. University of Cambridge. 254 pp.

Koenig, M., A.P. Monaco, and L.M. Kunkel. 1988. The complete sequence of dystrophin predicts a rod-shaped cytoskeletal protein. *Cell.* 53:219–226.

Lee, M.P., S.D. Brown, A. Chen, and T.S. Hsieh. 1993. DNA topoisomerase I is essential in *Drosophila melanogaster. Proc. Natl. Acad. Sci. USA.* 90:6656–6660.

Lupas, A., M. Van Dyke, and J. Stock. 1991. Predicting coiled coils from protein sequences. *Science (Wash. DC)* 252:1162–1164.

Mermall, V., and K.G. Miller. 1995. The 95F unconventional myosin is required for proper organization of the *Drosophila* syncytial blastoderm. *J. Cell Biol.* 129:1575–1588.

Merrill, P.T., D. Sweeton, and E. Wieschaus. 1988. Requirements for autosomal gene activity during precellular stages of *Drosophila melanogaster. Development (Camb.)* 104:495–509.

Miller, K.G., and D.P. Kiehart. 1995. Fly division. *J. Cell Biol.* 131:1–5.

Miller, K.G., C.M. Field, and B.M. Alberts. 1989. Actin-binding proteins from *Drosophila* embryos: a complex network of interacting proteins detected by F-actin affinity chromatography. *J. Cell Biol.* 109:2963–2975.

Mount, S.M., C. Burks, G. Hertz, G.D. Stormo, O. White, and C. Fields. 1992. Splicing signals in *Drosophila*: intron size, information content, and consensus sequences. *Nucleic Acids Res.* 20:4255–4262.

Nolan, J.M., M.P. Lee, E. Wyckoff, and T.S. Hsieh. 1986. Isolation and characterization of the gene encoding *Drosophila* DNA topoisomerase II. *Proc. Natl. Acad. Sci. USA.* 83:3664–3668.

Pesacreta, T.C., T.J. Byers, R. Dubreuil, D.P. Kiehart, and D. Branton. 1989. *Drosophila* spectrin: the membrane skeleton during embryogenesis. *J. Cell Biol.* 108:1697–1709.

Postner, M.A., and E.F. Wieschaus. 1994. The *nullo* protein is a component of the actin-myosin network that mediates cellularization in *Drosophila melanogaster* embryos. *J. Cell Sci.* 107:1863–1873.

Postner, M.A., K.G. Miller, and E.F. Wieschaus. 1992. Maternal effect mutations of the sponge locus affect actin cytoskeletal rearrangements in *Drosophila melanogaster* embryos. *J. Cell Biol.* 119:1205–1218.

Rabinowitz, M. 1941. Studies on the cytology and early embryology of the egg of *Drosophila melanogaster. J. Morphol.* 69:1–49.

Roberts, D.B. 1986. *Drosophila*: a practical approach. *In* Practical Approach Series. D. Rickwood and B.D. Hames, editors. IRL Press, Oxford, UK. 59–81.

Robertson, H.M., C.R. Preston, R.W. Phillis, D.M. Johnson-Schlitz, W.K. Benz, and W.R. Engels. 1988. A stable genomic source of P element transposase in *Drosophila melanogaster. Genetics.* 118:461–470.

Sambrook, J., E.F. Fritsch, and T. Maniatis. 1989. Molecular Cloning: A Laboratory Manual. Cold Spring Harbor Laboratory, Cold Spring Harbor, NY. 545 pp.

Schejter, E.D., and E. Wieschaus. 1993. Functional elements of the cytoskeleton in the early *Drosophila* embryo. *Annu. Rev. Cell Biol.* 9:67–99.

Schejter, E.D., L.S. Rose, M.A. Postner, and E. Wieschaus. 1992. Role of the zygotic genome in the restructuring of the actin cytoskeleton at the cycle-14 transition during *Drosophila* embryogenesis. *Cold Spring Harbor Symp. Quant. Biol.* 57:653–659.

Sheets, M.D., S.C. Ogg, and M.P. Wickens. 1990. Point mutations in AAUAAA and the poly (A) addition site: effects on the accuracy and efficiency of cleavage and polyadenylation in vitro. *Nucleic Acids Res.* 18:5799–5805.

Studier, F.W., A.H. Rosenberg, J.J. Dunn, and J.W. Dubendorff. 1990. Use of T7 RNA polymerase to direct expression of cloned genes. *Methods Enzymol.* 185:60–89.

Sullivan, W., J.S. Minden, and B.M. Alberts. 1990. *daughterless-abo-like*, a *Drosophila* maternal-effect mutation that exhibits abnormal centrosome separation during the late blastoderm divisions. *Development (Camb.).* 110: 311–323.

Sullivan, W., P. Fogarty, and W. Theurkauf. 1993. Mutations affecting the cytoskeletal organization of syncytial *Drosophila* embryos. *Development (Camb.).* 118:1245–1254.

Suzuki, A., M. Yoshida, H. Yamamoto, and E. Ozawa. 1992. Glycoprotein-binding site of dystrophin is confined to the cysteine-rich domain and the first half of the carboxy-terminal domain. *FEBS Lett.* 308:154–260.

Thomas, G.H., and D.P. Kiehart. 1994. Beta heavy-spectrin has a restricted tissue and subcellular distribution during *Drosophila* embryogenesis. *Development (Camb.).* 120:2039–2050.

Wagner, K.R., J.B. Cohen, and R.L. Huganir. 1993. The 87K postsynaptic membrane protein from *Torpedo* is a protein-tyrosine kinase substrate homologous to dystrophin. *Neuron.* 10:511–522.

Warn, R.M., R. Magrath, and S. Webb. 1984. Distribution of F-actin during cleavage of the *Drosophila* syncytial blastoderm. *J. Cell Biol.* 98:156–162.

Wieschaus, E., and D. Sweeton. 1988. Requirements for X-linked zygotic gene activity during cellularization of early *Drosophila* embryos. *Development (Camb.).* 104:483–493.

Young, P.E., T.C. Pesacreta, and D.P. Kiehart. 1991. Dynamic changes in the distribution of cytoplasmic myosin during *Drosophila* embryogenesis. *Development (Camb.).* 111:1–14.

Zalokar, M. 1976. Autoradiographic study of protein and RNA formation during early development of *Drosophila* eggs. *Dev. Biol.* 49:425–437.